Computational and Structural Biotechnology Journal 23 (2024) 2763–2778

Contents lists available at ScienceDirect

Computational and Structural Biotechnology Journal

journal homepage: www.elsevier.com/locate/csbj

Advancing PFAS risk assessment: Integrative approaches using agent-based modelling and physiologically-based kinetic for environmental and health safety

Martina Iulini [a,1], Giulia Russo [b,1], Elena Crispino [c,1], Alicia Paini [d], Styliani Fragki [d], Emanuela Corsini [a], Francesco Pappalardo [b,*]

[a] Università degli Studi di Milano, Department of Pharmacology and Biomolecular Sciences 'Rodolfo Paoletti', Milan, Italy
[b] University of Catania, Department of Drug and Health Sciences, Italy
[c] University of Catania, Department of Biomedical and Biotechnological Sciences, Italy
[d] esqLABS GmbH, Saterland, Germany

ARTICLE INFO

Keywords:
Per- and polyfluoroalkyl substances (PFAS)
Immunotoxicity
Risk assessment
Agent-based modeling
Physiologically based kinetic modeling

ABSTRACT

Per- and polyfluoroalkyl substances (PFAS), ubiquitous in a myriad of consumer and industrial products, and depending on the doses of exposure represent a hazard to both environmental and public health, owing to their persistent, mobile, and bio accumulative properties. These substances exhibit long half-lives in humans and can induce potential immunotoxic effects at low exposure levels, sparking growing concerns. While the European Food Safety Authority (EFSA) has assessed the risk to human health related to the presence of PFAS in food, in which a reduced antibody response to vaccination in infants was considered as the most critical human health effect, a comprehensive grasp of the molecular mechanisms spearheading PFAS-induced immunotoxicity is yet to be attained. Leveraging modern computational tools, including the Agent-Based Model (ABM) Universal Immune System Simulator (UISS) and Physiologically Based Kinetic (PBK) models, a deeper insight into the complex mechanisms of PFAS was sought. The adapted UISS serves as a vital tool in chemical risk assessments, simulating the host immune system's reactions to diverse stimuli and monitoring biological entities within specific adverse health contexts. In tandem, PBK models unravelling PFAS' biokinetics within the body i.e. absorption, distribution, metabolism, and elimination, facilitating the development of time-concentration profiles from birth to 75 years at varied dosage levels, thereby enhancing UISS-TOX's predictive abilities. The integrated use of these computational frameworks shows promises in leveraging new scientific evidence to support risk assessments of PFAS. This innovative approach not only allowed to bridge existing data gaps but also unveiled complex mechanisms and the identification of unanticipated dynamics, potentially guiding more informed risk assessments, regulatory decisions, and associated risk mitigations measures for the future.

1. Introduction

Per- and polyfluoroalkyl substances (PFAS) are a group of thousands of manmade chemicals widely used in many consumers and industrial products, which people and environment are exposed to. PFAS can be found in a wide range of products such as non-stick cookware, water-repellent clothing, stain-resistant fabrics and carpets, some cosmetics, and products that resist grease, water, and oil. Their widespread use and persistence in the environment make PFAS contamination a concern for food safety as well. Although production of certain PFAS was discontinued in the EU for more than 20 years, measurable blood concentrations have still been recorded in populations worldwide (EFSA Panel on Contaminants in the Food Chain [1]. The eight-carbon substances, perfluorooctane sulfonate (PFOS) and perfluorooctanoic acid (PFOA), are the most well-studied chemicals of the group with regards to their toxicity profile and toxicokinetic. Considering toxicokinetic of PFAS, there are species-, as well as gender-specific differences, mainly related to their elimination half-lives, intra-hepatic and intra-renal concentrations and excretion patterns [2]. PFAS are relatively well-absorbed after oral ingestion in mammals and humans and are

* Corresponding author.
E-mail address: francesco.pappalardo@unict.it (F. Pappalardo).
[1] Equal contribution.

https://doi.org/10.1016/j.csbj.2024.06.036
Received 30 April 2024; Received in revised form 28 June 2024; Accepted 28 June 2024
Available online 1 July 2024

taken up by the gut entering as such into the systemic circulation. Distribution occurs in plasma and different parts of the body. While this article focuses on oral exposure, it should be recognized that there are other routes of exposure to PFAS beyond oral ingestion, including inhalation of contaminated air and dust and dermal absorption, which are particularly relevant to workers in industries such as manufacturing, fire prevention and chemical processing [3]. PFAS do not undergo any metabolism, whereas precursors, like fluorotelomer alcohols and polyfluoroalkyl phosphate esters are broken down to several metabolites, including perfluoroalkyl carboxylic acids [1]. From the gut, they are transported to the liver by the portal blood. Elimination is mainly via urinary excretion in most species, while fecal excretion is less investigated. Although PFAS (mainly PFOS and PFOA) were shown to be excreted in the bile, it is believed that most of the amounts (>97 %) appearing in the gastrointestinal tract are extensively re-absorbed and enter into the enterohepatic cycle [4,5]. On the other hand, re-absorption via kidney transporters has been well-studied [6–8]. Both (intestinal and renal) re-absorption processes are thought to play a key role in the long elimination of half-lives of PFAS in humans. For example, the estimated mean half-life in humans is 5.3 years (95 % CI 4.6 to 6.0) for perfluorohexanesulfonic acid (PFHxS), 3.4 years (95 % CI 3.1 to 3.7) for PFOS and 2.7 years (95 % CI 2.5 to 2.9) for PFOA [9]. Epidemiology and laboratory studies have shown that PFAS are immunotoxic at low exposure levels and they can affect both cell-mediated and humoral immunity [1,10]. Reported effects of PFAS in laboratory animals include decreased spleen and thymus weights and cellularity and altered cytokine production. Elevated PFAS blood levels were associated with lower antibody responses to vaccinations in children [11] and in adults [12]. In addition, some studies reported a correlation between PFAS levels in the body and lower resistance to disease or an increased risk of infections [13]. A relationship between higher PFAS levels and increased risk of asthma [14] as well as increased adolescent food allergies [15] were also reported. The European Food Safety Authority (EFSA) has assessed the risk to human health related to the presence of PFAS in food and considered the reduced antibody response to vaccination in one-year-old children as the most critical human health effect. A tolerable weekly intake (TWI) threshold of 4.4 ng/kg body weight per week was determined based on this critical effect for the sum of four PFAS (PFOA, PFOS, perfluorononaoic acid: PFNA and PFHxS), representing the most abundant PFAS in human serum. [1]. However, a full understanding of the molecular mechanisms leading to PFAS-induced immunotoxicity has not yet been established.

Modelling and simulation are gradually gaining interest as critical tools for safety and risk assessment of a variety of compounds including drugs, chemicals, consumer products, and food ingredients. Recently, the agent-based model (ABM) Universal Immune System Simulator (UISS) was repurposed to inform chemical risk assessment and in particular it was extended and applied to a case study on allergic contact dermatitis, considering nickel as a skin sensitizer able to induce an immune response that was correctly simulated by UISS implementing UISS-TOX that is specifically tailored for predicting immunotoxicity [16,17]. The UISS computational framework facilitates the simulation of the host immune system's reaction to various stimuli. This framework permits the tracking of individual biological entities within a specific adverse health context, along with their immunological interrelations. Furthermore, this approach fosters the emergence of complex behaviors, potentially resulting in the identification of unanticipated dynamics.

Physiologically based kinetic (PBK) models have been used to simulate chemical kinetics taking into account the absorption, distribution, metabolism, and elimination processes that govern the fate and transport of the chemical in the body [18]. PBK models use differential equations to describe these processes in the body and are represented as a series of interconnected compartments linked via blood flow, to simulate concentration-time curves in target organs or their surrogates, e.g blood [19]. The use of PBK models helps to reduce uncertainties and to identify data gaps inherent in hazard characterization approaches. PBK models provide a sound scientific basis to extrapolate across species, routes of exposure, and exposure scenarios, based on species-specific physiology and substance-specific (physico-)chemical properties [20,21]. Next to this they can facilitate quantitative in vitro to in vivo extrapolation reverse dosimetry approaches, enabling the use and interpretation of in vitro toxicity data [22,23].

In the current study the existing PFAS PBK models were used to simulate time concentration profiles, from birth to 75 years, at different doses to inform UISS-TOX. The aim of the paper is to demonstrate how the employment of cutting-edge computational methodologies, particularly the ABM, UISS-TOX and the PBK models, has significantly deepened our understanding of the intricate ways in which PFAS interact with and affect the human immune system. These innovative tools offer a robust framework for simulating how the immune system reacts to various environmental stimuli, allowing for the precise tracking of biological entities and their responses in situations that pose a health risk. Moreover, they provide a comprehensive model for understanding the biokinetics of PFAS - encompassing absorption, distribution, metabolism, and elimination processes - thereby enabling the generation of detailed profiles that illustrate the concentration of these substances in the human body from birth through to advanced age.

2. Methodology

2.1. Physiological Based Kinetic (PBK) model for PFAS - selection

Several PBK models for PFAS, especially PFOA and PFOS, have been developed and are available in the literature. The Thompson PBK model database [24] and search engines were used to search for available PFAS-PBK models, resulting in 16 human PBK models available for PFOA and 11 for PFOS. In addition, EFSA published a revised PBK model code for PFOA and PFOS in 2020 [1],. based on an earlier model developed by Loccisano et al. [25] [1]. Further details on the models used can be found in the EFSA opinion appendix M on PBPK modelling – model description [1]. The PBK models of PFOA and PFOS were extended in order to describe the biokinetics of PFNA and PFHxS respectively, based on information on their reported elimination half-lives [in accordance with 26]. In particular, the PBK models were re-scaled with respect to the PBK transporter maximum capacity for renal tubular reabsorption in order to reach the reported human elimination half-lives of PFNA and PFHxS. Mean elimination half-lives of 3.2 and 8.2 years were applied for PFNA and PFHxS [27,28]. Prior to the renal reabsorption changes, tissue: blood partition coefficients were adapted for the liver and kidney for both PFNA and PFHxS (original references reported; Tables 2 and 3). In the tables below (Table 2 and Table 3) the input parameters for PFNA and PFHxS are shown. The PFAS PBK models were used here as such, and no PBK model development was performed as part of the present study. We describe below the models following the OECD PBK model guidance document (GD331).

2.1.1. PBK model input parameters

The input parameters were based on the EFSA PBK models [1,29], and Table 1 reports the used values for the selected PFAS: PFOA and PFOS. PFAS poses challenges to conventional models based on octanol-water partitioning, which are not applicable here, requiring specific partitioning approaches [30,31] or generation of ad hoc measured data. Chemical-specific parameters used were the distribution partition coefficients, the plasma protein binding, as well as the parameters related to urinary elimination and re-absorption. The tissue-plasma partition coefficients were derived from animal data (in rodents, rat or mouse), and as such there is some uncertainty pertaining to their application. An alternative to these parameters would be the application of tissue-blood partition coefficients, which are based on human data [32,33], as estimated by Fàbrega et al. [34]. However, due to variation in studies design and data gaps, it was considered more appropriate to use the animal-based partition coefficients. For the free

Table 1
Parameters applied to the PBK model for PFOS and PFOA.

Input Parameters	Values	Reference
Integration method	Rosenbrock (Stiff)	EFSA CONTAM PANEL, 2018 [29]
DT min	1.00E-06	EFSA CONTAM PANEL, 2018 [29]
DT max	10	EFSA CONTAM PANEL, 2018 [29]
DT	0.01	EFSA CONTAM PANEL, 2018 [29]
Tolerance	0.01	EFSA CONTAM PANEL, 2018 [29]
PFOA		
Tmc; (μg/h/kg$^{0.75}$) Maximum resorption rate	6000	EFSA CONTAM PANEL, 2018 [29]
Kt; (μg/L) Resorption affinity	55	EFSA CONTAM PANEL, 2018 [29]
Free; Free fraction of PFOA in plasma	0.02	fit to plasma concentration in monkey (Loccisano et al., 2011) [25]
PL; Liver/plasma partition coefficient	2.2	Kudo et al., 2007 [36]
PF; Fat/plasma partition coefficient	0.04	Kudo et al., 2007 [36]
PK; Kidney/plasma partition coefficient	1.05	Kudo et al., 2007 [36]
PSk; Skin/plasma partition coefficient	0.1	Kudo et al., 2007 [36]
PR; Rest of the body/plasma partition coefficient	0.12	Kudo et al., 2007 [36]
PG; Gut/blood plasma coefficient	0.05	Kudo et al., 2007 [36]
Kurinec;urinary elimination rate constant (/h/kg^−0.25)	0.0003	estimated from Harada et al., (2005) [37]
PFOS		
Tmc; (μg/h/kg$^{0.75}$) Maximum resorption rate	3500	EFSA CONTAM PANEL, 2018 [29]
Kt; (μg/L) Resorption affinity	23	EFSA CONTAM PANEL, 2018 [29]
Free; Free fraction of PFOS in plasma	0.025	fit to plasma concentration in monkey (Loccisano et al. 2011) [25]
PL; Liver/plasma partition coefficient	3.72	de Pierre (Loccisano et al. 2011) [25]
PF; Fat/plasma partition coefficient	0.14	de Pierre (Loccisano et al. 2011) [25]
PK; Kidney/plasma partition coefficient	0.8	de Pierre (Loccisano et al. 2011) [25]
PSk; Skin/plasma partition coefficient	0.29	de Pierre (Loccisano et al. 2011) [25]
PR; Rest of the body/plasma partition coefficient	0.2	de Pierre (Loccisano et al. 2011) [25]
PG; Gut/blood plasma coefficient	0.57	de Pierre (Loccisano et al. 2011) [25]
Kurinec;urinary elimination rate constant (/h/kg^−0.25)	0.001	estimated from Harada et al. (2005) [37]

In the model for PFNA and PFHxS the tissue/blood partition coefficients were adjusted for liver and kidney according to Fragki et al. [26]. In the Tables 2 and 3 the input parameters for PFNA and PFHxS are reported as taken from Fragki et al. [26].

fraction (unbound) of chemicals, data were used from the species monkey [25], based on measured plasma concentrations. This was considered a valid approach, given that differences in PFAS half-lives amongst the species do not seem to specifically depend on protein binding [7]. PFAS elimination via urinary excretion and renal re-absorption is determined in the model using two main input parameters, the transporter maximum (Tm) where Tm = maximum resorption rate (Tmc) = Tmc*BW$^{0.75}$) and the transporter affinity constant (Kt). The Tmc and Kt values applied here were the same as those used earlier by EFSA [29], in order to reflect a half-life of 2.3 (3 years) and 5.4 (6 years) years, for PFOA [35] and PFOS [27] respectively.

Table 2
Models parameters to be considered for the PBK model simulations of PFNA.

PFNA Fragki et al. 2023[26]	
Tmc; (μg/h/kg$^{0.75}$) Maximum resorption rate	7900[a]
Kt; (μg/L) Resorption affinity	55
Free; Free fraction of PFNA in plasma, based on value for PFOA	0.02
PL; Liver/plasma partition coefficient	1.46[b]
PF; Fat/plasma partition coefficient	0.04
PK; Kidney/plasma partition coefficient	0.6[c]
PSk; Skin/plasma partition coefficient	0.1
PR; Rest of the body/plasma partition coefficient, based on value for PFOA	0.12
PG; Gut/blood plasma coefficient, based on value for PFOA	0.05
Kurinec;urinary elimination rate constant (/h/kg^−0.25); based on valued for PFOA	0.0003

[a] Calibrated to result in half-lives of 3.2 years (range: 0.34–20) for PFNA [27, 28].
[b] Original reference is [38].
[c] Original reference is [38].

Table 3
Models parameters to be considered for the PBK model simulations of PFHxS.

PFHxS	Fragki et al. 2023 [26]
Tmc; (μg/h/kg$^{0.75}$) Maximum resorption rate	7000[a]
Kt; (μg/L) Resorption affinity	23
Free; Free fraction of PFHxS in plasma, based on value for PFOS	0.025
PL; Liver/plasma partition coefficient	0.85[b]
PF; Fat/plasma partition coefficient, based on value for PFOS	0.14
PK; Kidney/plasma partition coefficient	0.3
PSk; Skin/plasma partition coefficient, based on value for PFOS	0.29[c]
PR; Rest of the body/plasma partition coefficient, based on value for PFOS	0.2
PG; Gut/blood plasma coefficient	0.57
Kurinec;urinary elimination rate constant (/h/kg^−0.25); based on value for PFOS	0.001

[a] Calibrated to result in half-lives of 8.2 years (range: 0.34–20) for PFHxS [27, 28].
[b] Original reference is [38].
[c] Original reference is [38].

2.1.2. PBK model codes and growth curves

Because EFSA developed, evaluated and applied the PFAS PBK model to set health-based guidance values, this published model was used. The PBK models were built in Berkely Madonna (BM) [39], and in the present study, the BM version 10.2.8 was used. The codes are available in the Supplementary Materials. The model structure (Fig. 1) represents the different life stages from birth, toddlers to adults, and depending on which population is modelled, the growth follows two curves from a French study [40], representing chronic exposure from birth to 50 years old and the WHO growth curves [41], available for girls and boys up to 5 years old. The French study included 4078 subjects (3 to 60 years), with 703 subjects of less than 3 years of age; from the reported data (weight, age) from this study, an equation describing the increase in weight according to age was included in the EFSA 2020 model.

2.1.3. PBK model representation of birth and breastfeeding

Birth and lactation models were included in the analysis. The placental transfer ratio for milk concentration/maternal serum PFAS concentration and the decline of PFAS in milk due to transfer to the infant are represented in the code. These models allow quantifying the initial amount of PFAS (e.g. PFOA) at birth and intake via breastfeeding in several compartments according to the maternal level at delivery and the placental transfer. In addition, the models provide a basis to predict the amount of PFOA in milk per month according to the milk concentration/maternal serum PFOA concentration ratio and the decline of PFOA in milk per month. The milk concentration/maternal serum concentration ratio, of 0.03 was used for PFOA and PFNA and of 0.015 for PFOS and PFHxS. The decline of PFAS concentration in milk per month

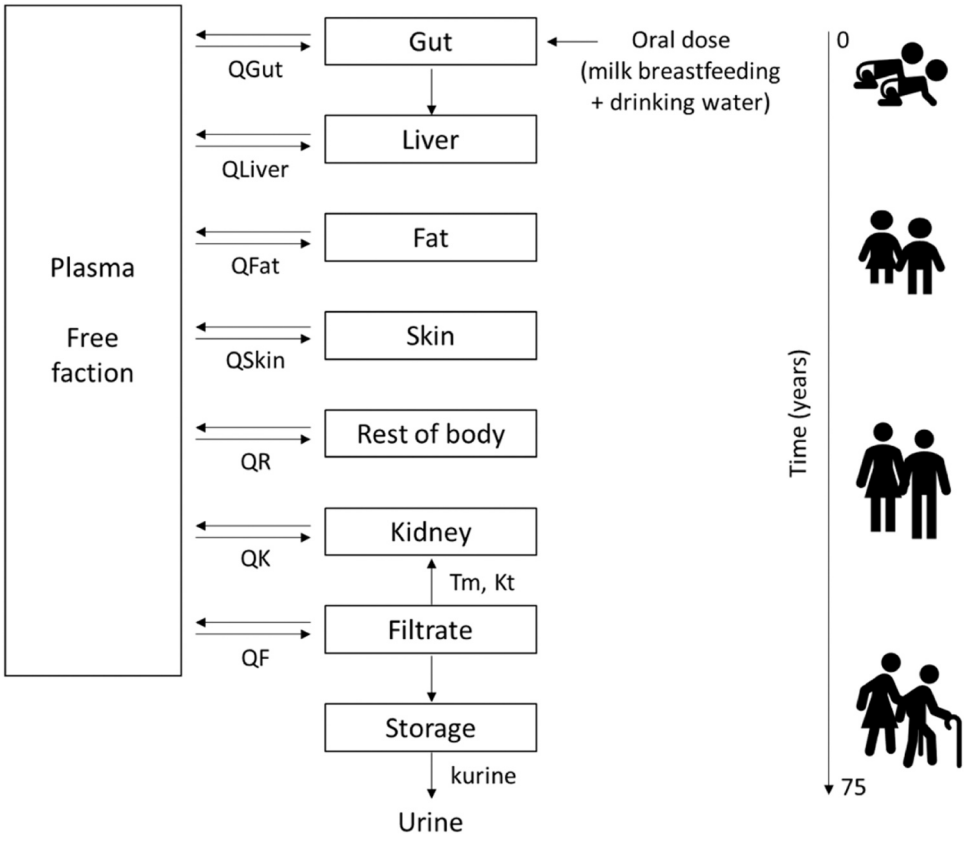

Fig. 1. PBK model representation figure modified from the EFSA CONTAM Panel (2018) [29] adapted from Loccisano et al. [25]. PFAS are taken up into the gut (oral). From the gut, chemical is transported to the liver by the portal blood. Only the free fraction of chemical in plasma is assumed to be available for partitioning into tissues. Chemical is eliminated through the filtrate compartment to storage into urine. While in the filtrate compartment, chemical can be reabsorbed back into the plasma through a saturable process with a transporter maximum Tm and affinity constant Kt. The Q indicate blood flows into and out of tissues. Q_F is not a blood flow, it is a clearance (L/h) from the plasma to the filtrate compartment.

was also introduced in the EFSA 2020 PBK model and a rate of 7.7 % per month was used for PFOA and PFNA, while a rate of 3.1 % per month was used for PFOS and PFHxS.

2.1.4. Sensitivity and uncertainty analyses

A sensitivity analysis was performed by EFSA and the results are reported in the EFSA 2020 opinion on PFAS [1]. Considering that no model development was performed here, an additional sensitivity analysis was considered to be outside the scope of this work.

2.1.5. Model evaluation

Model evaluation was performed earlier by EFSA to validate the PFOA and PFOS PBK model. A number of valid PBK models for PFOS and PFOA are available; a list of such models was already made in the EFSA Opinion [29]. Most of these models are built and validated using animal data, and in particular here the monkey PBK model from Loccisano et al., 2011 [25] was extrapolated to humans [29]. For both PFOA and PFOS, the chemical-specific input parameters used for the humans PBK models, such as the free fraction in plasma and the transporter affinity constant were those previously described for monkey [29], whereas tissue-plasma partition coefficients are from rodent (rat and mouse) tissue data. Transporter maximum capacity for renal tubular reabsorption is fitted in order to achieve the desired half-life in humans, which is higher compared to monkeys [25].

In the case of PFNA and PFHxS, tissue-blood partition coefficients were used for PFOA and PFOS, respectively, with the exception of liver and kidney, were data used were derived from rodent studies [approach followed as by 26]. Again here, transporter maximum capacity for renal tubular reabsorption is fitted in order to achieve the desired half-life in humans [26]. However, due to the absence of suitable human biomonitoring data, the PFNA and PFHxS models could not be verified directly on such data [26]. No further model validation for PFNA and PFHxS was performed here.

Physiology.based input parameters for the human model were those reported by Brown et al., 1997 [29,42]. Given that,the models do not include a separate tissue compartment for the immune systems and due to challenges pertaining to its parametrization and evaluation, the concentration in plasma was used as a surrogate. In particular the-concentration CA, which is the total concentration of chemicals in plasma (ng/ml), was modelled here.

2.1.6. PBK Model set up

The model was set up to include a long-life exposure to the PFAS, which was reflected to cover 75 years (0 to 75 years old), including exposure at birth and during breast feeding. Between WHO and French study, the latter option allows for modelling the lifetime exposure, while the WHO is reserved for toddlers up to 5 years of age. The model was then used to generate forward predictions based on selected exposure scenarios but also used in reverse dosimetry to reconstruct the exposure based on human biomonitoring data.

2.1.7. PBK modelled exposure scenarios – dose setting

Different scenarios of chronic oral exposure were then defined:

– Scenario 1 was set up to mimic the French study used in the EFSA 2020 scientific opinion on PFAS. In this opinion, PFOA and PFOS were simulated, and the other two PFAS (PFNA and PFHxS) were assumed to be similar. The doses used were PFOA and PFNA with an

oral exposure of 0.187 ng/kg day and PFOS and PFHxS with an oral exposure of 0.44 ng/kg day [1].
- Scenario 2. EFSA has set a safety threshold for the sum of four PFAS (PFOA, PFOS, PFNA and PFHxS) that can accumulate in the body. The group TWI of 4.4 ng/kg day – has been established following the assessment of the risks to human health arising from these substances in food. A daily intake was calculated by dividing the TWI (4.4 ng/kg day) by 7 days, resulting in 0.628 ng/kg day [1].
- Scenario 3 was based on food diet intake via oral exposure of 4.18 ng/kg day for PFOA, 3.68 ng/kg day for PFNA, of 3.45 ng/kg day for PFHxS and of 4.47 ng/kg day for PFOS, as found in populations that lived in high polluted areas (data extracted from the table 10 present in the EFSA Opinion 2020 [1].
- Scenario 4 was defined while applying the PBK models to recalculate exposure using reverse dosimetry and human biomonitoring (HBM) data (average age 42 years), with PFOA 8.6 ng/ml, PFOS 160 ng/ml and PFHxS 140 ng/ml concentration in blood [43].

2.2. UISS-TOX computational modeling infrastructure

The Universal Immune System Simulator (UISS) models the immune system using an agent-based approach within a bidimensional compartment. Each biological entity, including pathogens, cancer cells, and immune cells, is represented as an autonomous agent characterized by type, state, position, and interaction patterns. Chemical reactions within the system are defined by stoichiometric equations and occur stochastically, influenced by the proximity and concentration of chemical species. The agents follow specific interaction rules that dictate state transitions based on their current state, presentation pattern, and the local chemical environment. Agents can move randomly or in response to chemokine gradients and can appear or disappear based on these interactions. UISS operates from an initial configuration that evolves over time. Its nature is statistical, meaning different runs yield varied results, but repeated simulations approximate population averages. The entities, or "agents," are typically positioned within a simulation space known as a lattice, where multiple entities can occupy each lattice point. These agents can be diverse and possess internal properties such as lifetime, internal state, and energy. They can operate independently, moving, interacting with neighboring agents, altering their internal state, or dying, either on their own or due to interactions with other agents. Agent-based modeling (ABM) offers several advantages. By nature, it can be stochastic, incorporating delays and spatial descriptions, which allows for a more accurate representation of the biological characteristics and behaviors of the entities involved. Therefore, the precision of the description is more often constrained by biological understanding than by the modeling approach. Nonlinear behaviors and the ability to integrate additional complexity and biological insights are easily handled within the model. These methods are also inherently numerically stable since most variables are represented as integers, requiring minimal complex floating-point calculations. UISS is programmed entirely in ANSI C-99, ensuring it is platform-independent. It incorporates both cellular and molecular entities, typically tracking cellular entities individually and modeling them as distinct agents. In contrast, molecular entities are represented by their concentration at each lattice site. Cellular agents possess properties like position, half-life, and an internal state from a defined set of states, with their dynamics governed by state changes triggered by interactions with other agents, whether cells or molecules. Cellular entities such as B and T lymphocytes, macrophages, and dendritic cells are modeled individually, while molecules like interleukins and immunoglobulins are represented by their concentrations. The model also incorporates key immune functions such as clonal selection, thymus education, antigen processing, and immune memory. Interactions, essential for state changes, occur within a defined lattice-space that can be 2D or 3D, with agents moving according to Brownian motion. These interactions are modeled as Bernoulli events with specific and aspecific reactions. Specific interactions, particularly for adaptive immunity, require receptor-ligand recognition, modeled using bit-strings and Hamming distance for affinity. The simulation includes processes like hematopoiesis and thymus selection to ensure a repertoire of functional immune cells. Time in UISS is discrete, with activities measured at set intervals. Interactions are complex and depend on physical proximity within the lattice. The initialization phase populates the lattice, and simulations proceed through synchronized time-steps. UISS's core features are stable, but extensions can be added to model specific pathologies, ensuring flexibility and accuracy in representing biological mechanisms. UISS works with a multi-layer approach, taking into account:

- The physiological activity and response of the immune system to a non-self (or self in the presence of autoimmune disease) entity (physiology layer);
- The dynamics related to the progression of a disease (disease layer);
- Eventually, the effects induced by different treatments, including vaccines, on the control of the disease (treatment layer).

The PFAS disease layer has already been integrated into UISS [16], resulting in UISS-TOX, which can model the effects of PFOA/PFOS on the immune system. To build the UISS-TOX disease layer within UISS, we began by gathering data from the literature and translating it into a conceptual model, which serves as a schematic representation of all entities and interactions involved in the mechanisms by which PFOA and PFOS affect the immune system. The following step consisted of the implementation of the mechanism of action of PFAS and, finally, the UISS simulation to predict how these substances affect the immune system activity and responses.

2.3. PBK model inter-operability with UISS-TOX

In order to make the PBK model inter-operable with the UISS-TOX, the interval of CA every 8 h was chosen and the data was extracted in excel format and used to inform the UISS-TOX (results not shown). Here, we used the PK/PD model described above to input UISS-TOX with three different concentrations of PFOA and PFOS in three different populations (children, young people, and elderlies) to predict the effects on the human immune system response in two different circumstances: i) a generic bacterial challenge and ii) the immune response to two widely used vaccinations (anti-H1N1 and anti-diphtheria).

3. Results

3.1. Simulation PBK results with forward dosimetry

The first simulations mimicked the French study (scenario 1) in the EFSA 2020 scientific opinion on PFAS. The four PFAS: PFOA, PFNA, PFHxS and PFOS were simulated. The doses used were PFOA (A) and PFNA (C) with an oral exposure of 0.187 ng/kg day and PFHxS (D) and PFOS (B) with an oral exposure of 0.44 ng/kg day. The results are presented in Fig. 2.

Scenario 2 was taken from the EFSA TWI of 4.4 ng/kg day for the main PFAS, that accumulate in the body [1]. A daily intake of 0.628 ng/kg day was calculated by dividing the TWI (4.4 ng/kg day) by 7 days and simulation results are shown in Fig. 3.

The scenario 3 is based on food diet intake level and was selected to represent a worst-case scenario (WSC). The data were extracted from table 10 of the EFSA Opinion on PFASs [1], which reported food diet intake in populations that lived in high polluted areas. The table reported median upper boundary chronic dietary exposures of 4.18 ng/kg day for PFOA (A), of 3.68 ng/kg day for PFNA (C), of 3.45 ng/kg day for PFHxS (D) and of 4.47 ng/kg day for PFOS (B). The results are represented in Fig. 4.

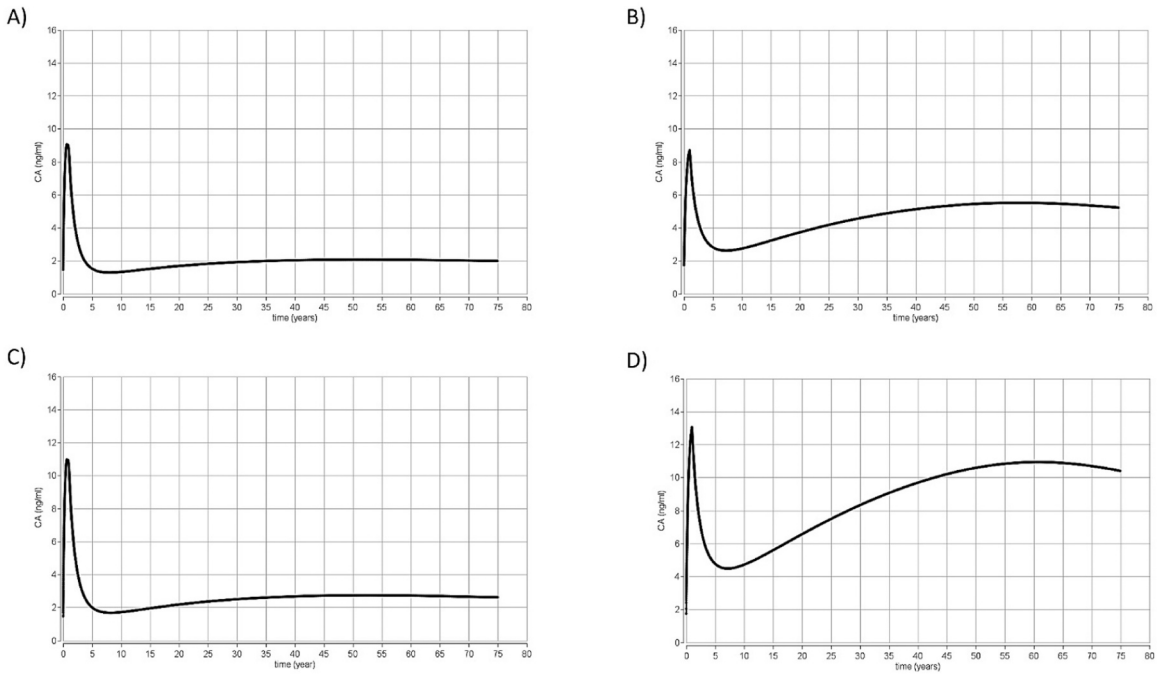

Fig. 2. Simulation scenario 1. Results from time concentration simulations using the PBK models for the four PFAS from birth to 75 years old (EFSA CONTAM 2020) for exposure to (A) PFOA and (C) PFNA with an oral exposure of 0.187 ng/kg/day and (B) PFOS and (D) PFHxS with an oral exposure of 0.444 ng/kg/day. CA represents the total concentration of chemical in blood (ng/ml) (Y axis) and the time is expressed in years (x axis).

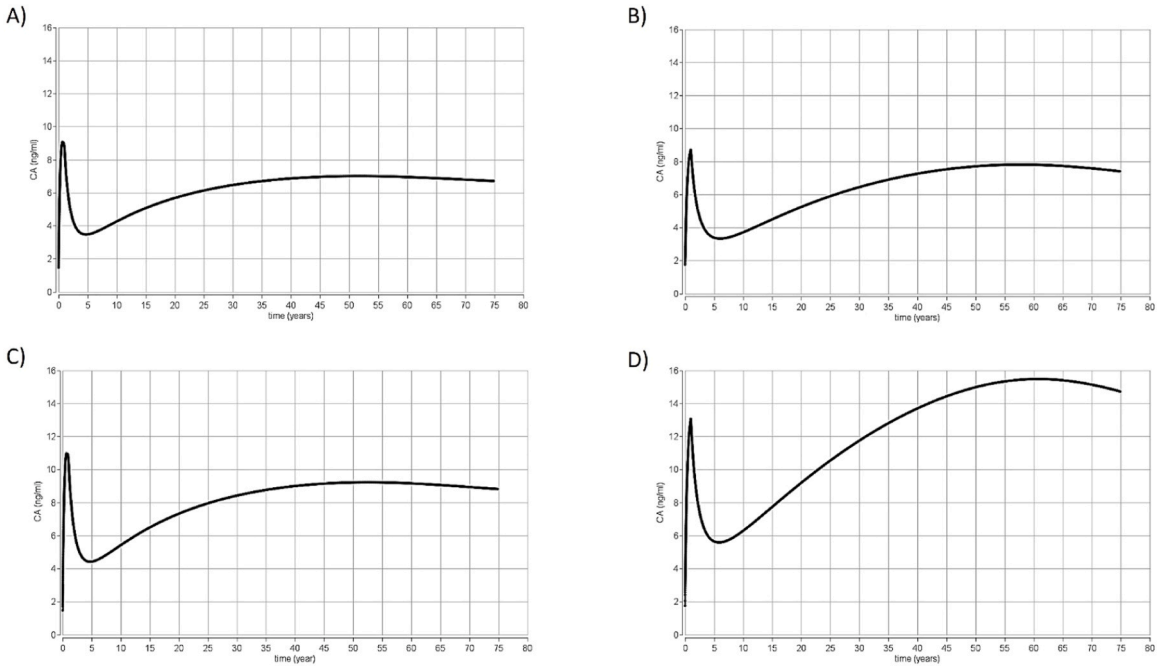

Fig. 3. Scenario 2. Results from time concentration simulations using the PBK models for the four PFAS from birth to 75 years old (EFSA 2020 model) for exposure to (A) PFOA, (B) PFOS, (C) PFNA and (D) PFHxS all with an oral exposure of 0.628 ng/kg/day. This dose was selected as the oral exposure estimate from the EFSA 2020 TWI of 4.4 ng/kg. CA represents the total concentration of chemical in blood of the chemicals (ng/ml) (Y axis) and the time is expressed in years (x axis).

3.2. Simulations PBK results with reverse dosimetry

In scenario 4, reverse dosimetry was performed using the PBK models while applying them to human biomonitoring (HMB) data to reconstruct and estimate the exposure. HBM data were taken from Li et al. [43] who reported the plasma concentration of several PFAS in the blood of 1815 Swedish adults exposed to contaminated water. The average age of the adult population was 42 years (adults from 20 to 60 years), and the results indicated that the serum concentration for PFOA was 8.6 ng/ml, for PFHxS 160 ng/ml and for PFOS was 160 ng/ml. The results obtained from the reverse dosimetry are reported below in Fig. 5. This resulted in the following predictions with regards to continuous oral exposure: (A) 0.8 ng PFOA/kg/day (B) 13.6 ng PFOS/kg/day and (C) 6.3 ng PFHxS/kg/day.

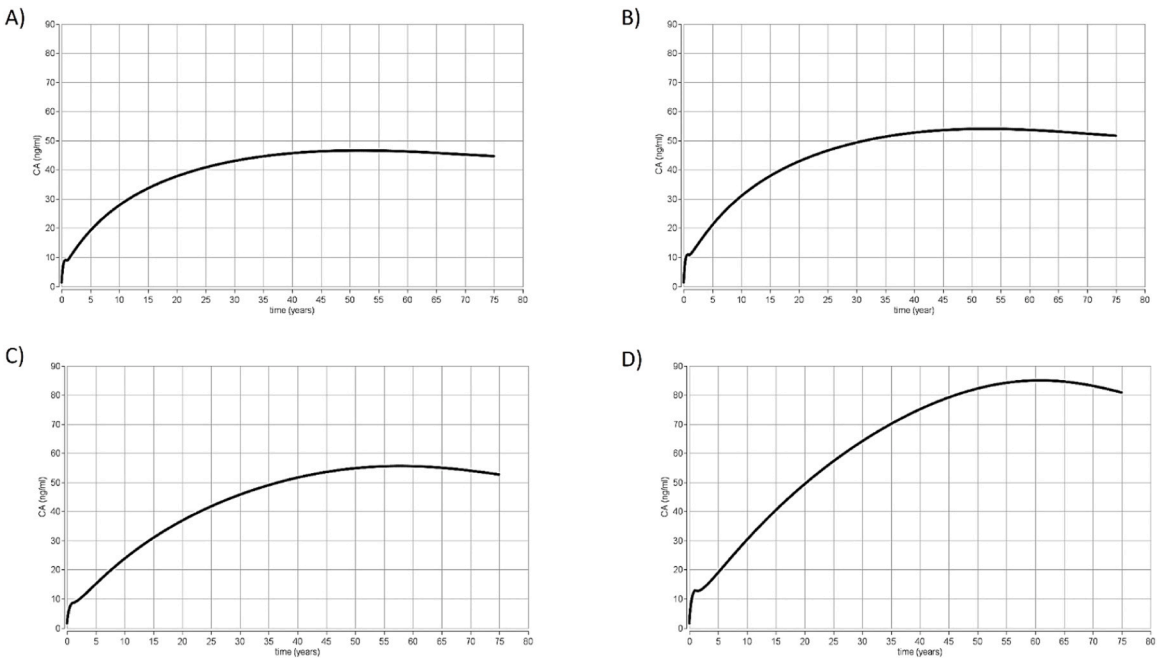

Fig. 4. Scenario 3. Results from time concentration simulations using the PBK models for the four PFAS from birth to 75 years old (EFSA CONTAM 2020) for exposure to (A) PFOA with an oral exposure of 4.18 ng/kg/day, (B) PFOS with an oral exposure of 4.47 ng/kg/day, (C) PFNA with an oral exposure of 3.68 ng/kg/day and (D) PFHxS with an oral exposure of 3.45 ng/kg/day. This dose was selected to represent a worst-case scenario (WCS) data were taken table 10 (present in the EFSA CONTAM 2020 [1]) in which the mean upper bound was selected. CA represents the total concentration of chemical in blood (ng/ml) (Y axis) and the time is expressed in years (x axis).

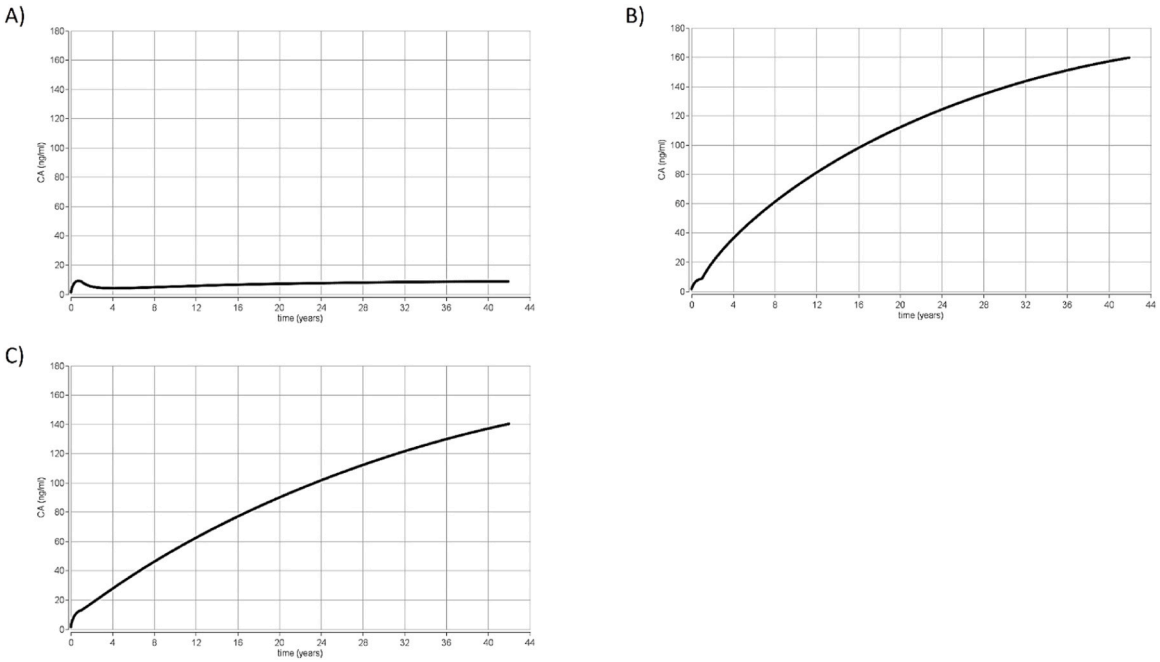

Fig. 5. Scenario 4. Results from time concentration simulations using the PBK models for (A) PFOA, (B) PFOS and (C) PFHxS. The PBK models were used to predict the time concentration profile curve with a continuous exposure up to 42 years, based on blood levels of 8.6 PFOA ng/ml, 160 PFOS ng/ml and 140 PFHxS ng/ml, in order to estimate the external exposure. CA represents the total concentration of chemical in blood (ng/ml) (Y axis) and the time is expressed in years (x axis).

3.3. Results from UISS-TOX for the prediction of the response to vaccination for each scenarios considered 0-4 years (children); 25-26 years (young people); 65-66 years (elderlies)

The PFAS exposure scenarios described above (i.e., scenarios 1, 2, and 3) provided the chemical and immunological inputs that were used to feed the UISS-TOX platform. As a result, the *in silico* model was able to predict, according to three different age ranges and to three different scenarios, the immune system dynamic both from a cellular and humoral response point of view.

The considered three age ranges were:

- 0-4 years (children);
- 25-26 years (young people);

- 65-66 years (elderlies).

A general bacterial challenge was injected to each age group, and we subsequently examined the pro-inflammatory cytokines, antibodies, and B- and T-cell dynamics in the three different scenarios. Additionally, we modeled and predicted the antibody response following anti-H1N1 and anti-diphtheria vaccine injection in a young cohort of people (25–26 years) and according to the three different exposure scenarios.

– 0-4 years (children)

We simulated the immune system response after a generic bacterial challenge in young children (0–4 years old) exposed to three different concentrations of PFOA and PFOS coming from the PBK model, evaluating their immune response in terms of cytokine, immunoglobulins, and B- and T-cells dynamics.

Here, we show the cytokines and immunoglobulins dynamics prediction for digital patients in the age range 0–4 years old, unexposed, and exposed to PFOA and PFOS according to "scenario 3". Results obtained for the B- and T-cells immune dynamics and the other scenarios (i.e., scenario 1 and scenario 2), are presented in Supplementary Materials.

Fig. 6 and Fig. 7 show IL-2, IL-6, TNF-α, and IL-17 dynamics in unexposed children and in exposed children according to "scenario 3″, respectively.

From the comparison of Fig. 7 (PFOA and PFOS exposure, scenario 3) with Fig. 6 (PFAS unexposed), it can be appreciated that the cytokine concentration levels decrease in scenario 3. This behavior reflects the data of the literature, i.e. PFAS induce a reduction in IL-2, IL-6, TNF-α, and IL-17 [44,45]. It is important to note that IL-6 promotes the differentiation of T lymphocytes into CD4 and CD8; hence, through a reduction of IL-6, PFAS may be responsible for altering T-cell populations, particularly CD4 and CD8, as we can see in the plots depicting the dynamics of T and B cells that are shown in Supplementary Materials.

Fig. 8 and Fig. 9 show the immunoglobulins dynamics, particularly the IgM and IgA levels, in young children (0–4 years old) unexposed and exposed to PFOA and PFOS according to the "scenario 3″, respectively.

The immunoglobulin concentration gradually decreases along with the three scenarios, as we can also see in the plots representing IgM and IgA dynamics of the scenarios 1 and 2, which are shown in Supplementary Materials. Comparing Fig. 9 (PFOA and PFOS exposure, "scenario 3″) and Fig. 8 (PFAS not exposed), we can see that the immunoglobulin concentration levels are much lower in children exposed to PFOA and PFOS than in unexposed ones. In fact, a reduction in antibody levels is one of most significant consequences that PFAS have on humoral response.

– 25-26 years (young people)

We simulated the immune system response after a generic bacterial challenge in digital patients aged 25–26 (young people) who were previously unexposed and exposed to the different concentrations of PFOA and PFOS coming from the three PBK model scenarios. We evaluated the immune response considering the cytokines, immunoglobulins, and T- and B-cells dynamics. T- and B-cells dynamics are shown in Supplementary Materials.

Fig. 10 and Fig. 11 show the cytokine concentration levels in unexposed young people and exposed ones according to the "scenario 3″, respectively. From the comparison of the Figures, also considering the ones representing the cytokine dynamics in the scenarios 1 and 2 (shown in Supplementary Materials), one can appreciate that the cytokine concentration levels will gradually decrease along with the three scenarios.

Figs. 12 and 13 depict the IgM and IgA dynamics in unexposed young

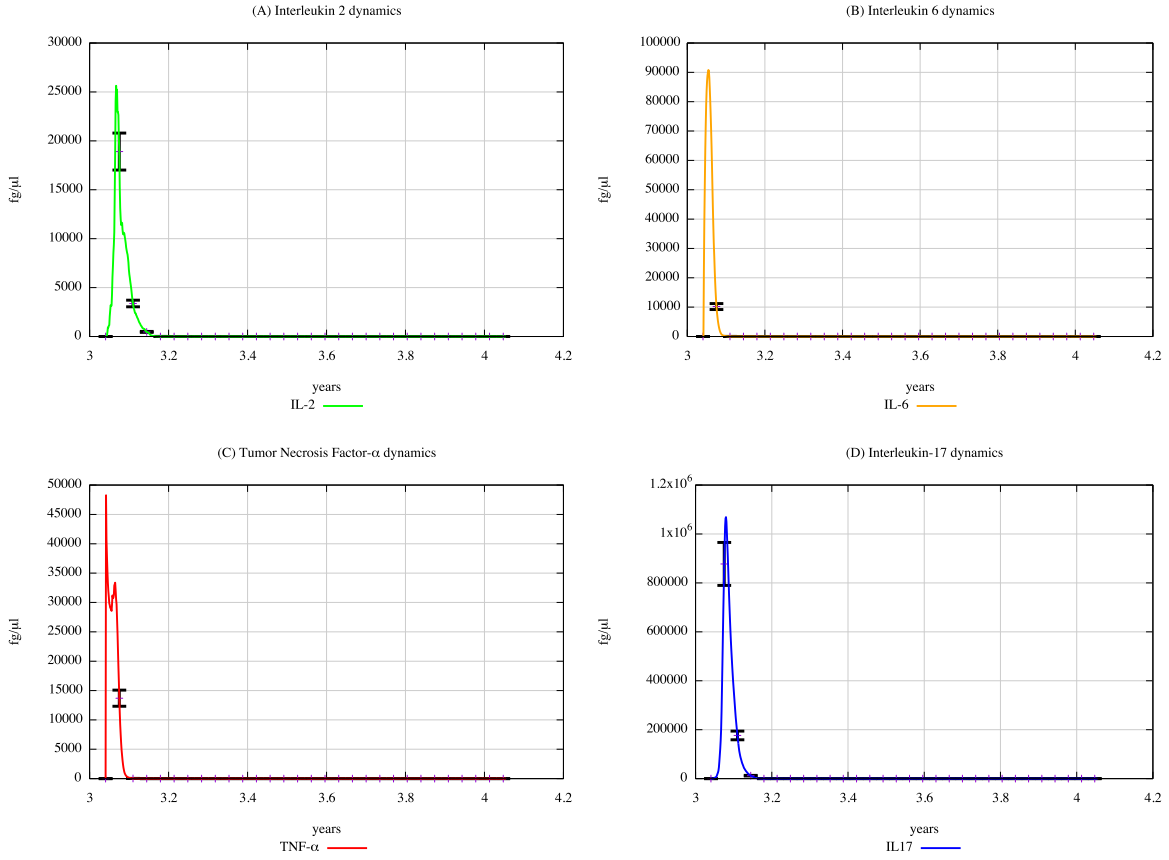

Fig. 6. Cytokines dynamics prediction for "not exposed" scenario, age range 0–4 years.

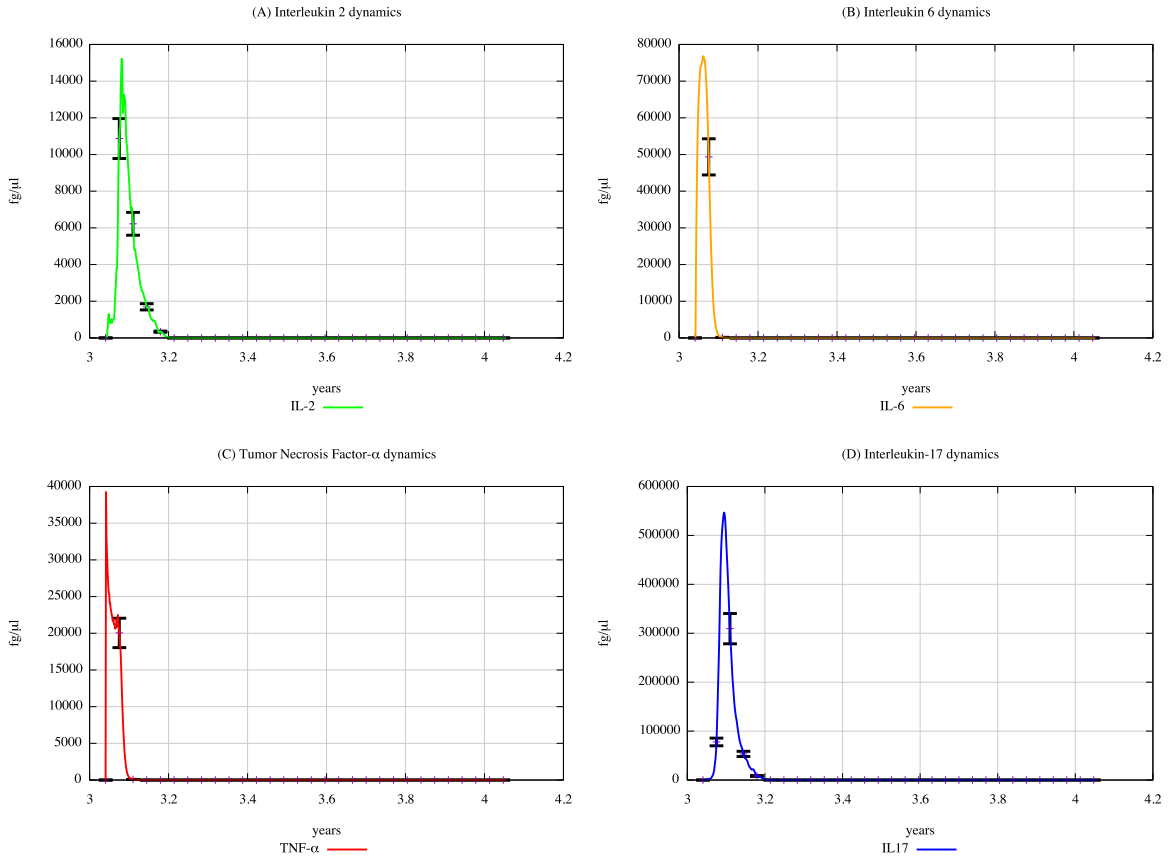

Fig. 7. Cytokines dynamics prediction for a digital cohort having an age range of 0–4 years and exposed to PFOA and PFOS according to "scenario 3″.

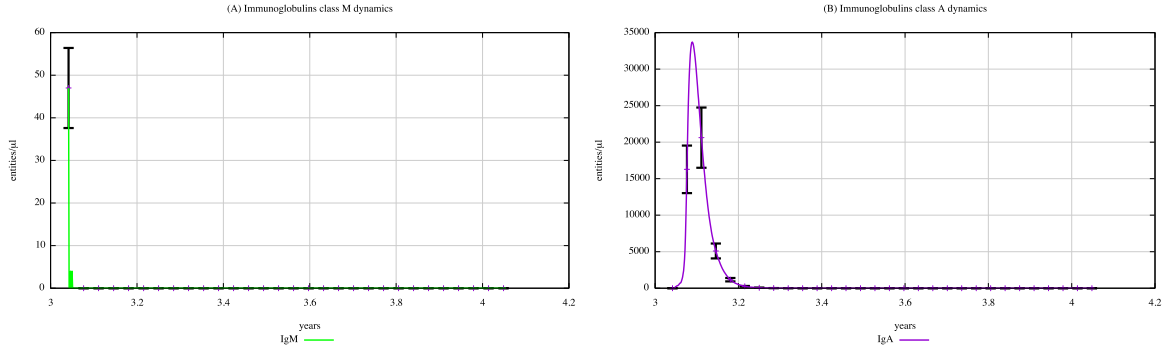

Fig. 8. Immunoglobulins dynamics prediction for "not exposed" scenario, age range 0–4 years.

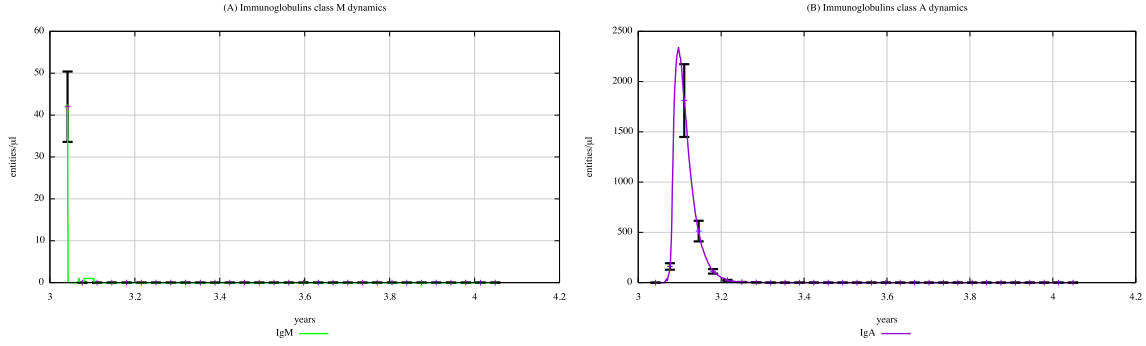

Fig. 9. Immunoglobulins dynamics prediction for a digital cohort having an age range of 0–4 years and exposed to PFOA and PFOS according to "scenario 3″.

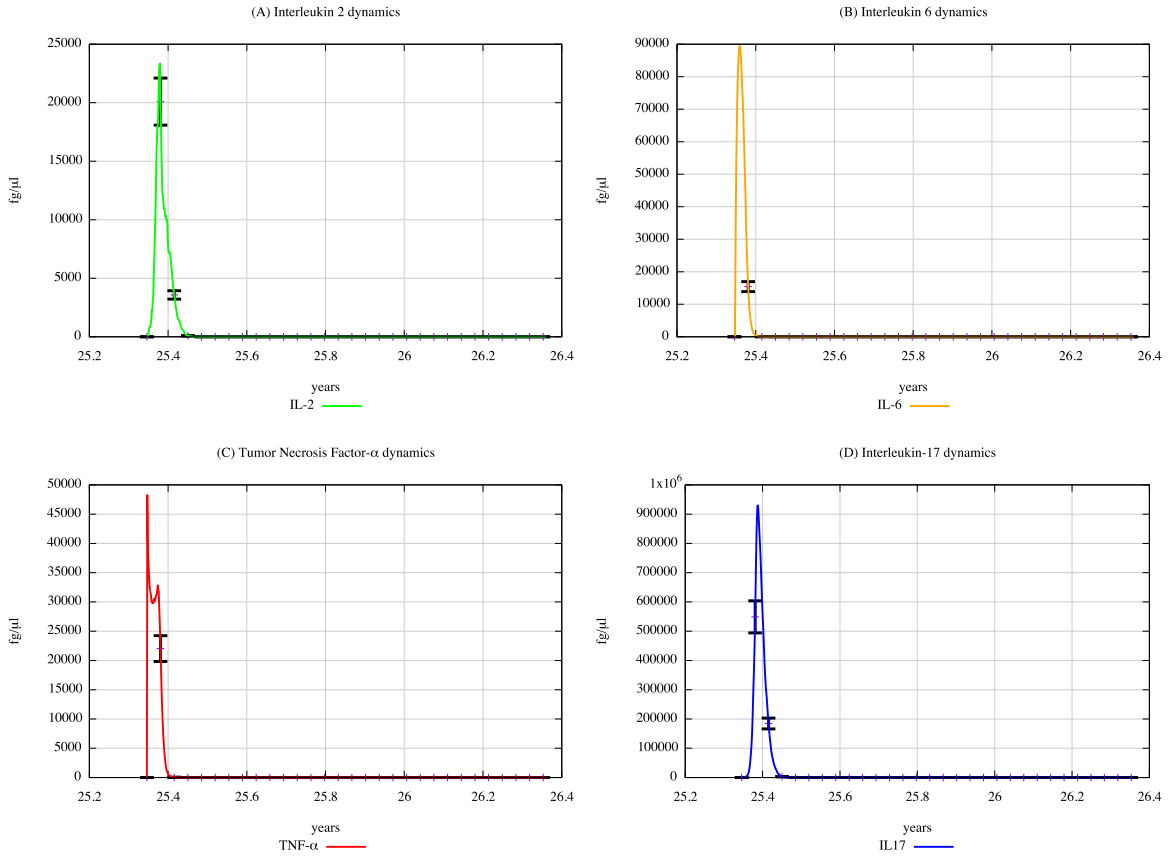

Fig. 10. Cytokines dynamics prediction for "not exposed" scenario, age range 25–26 years.

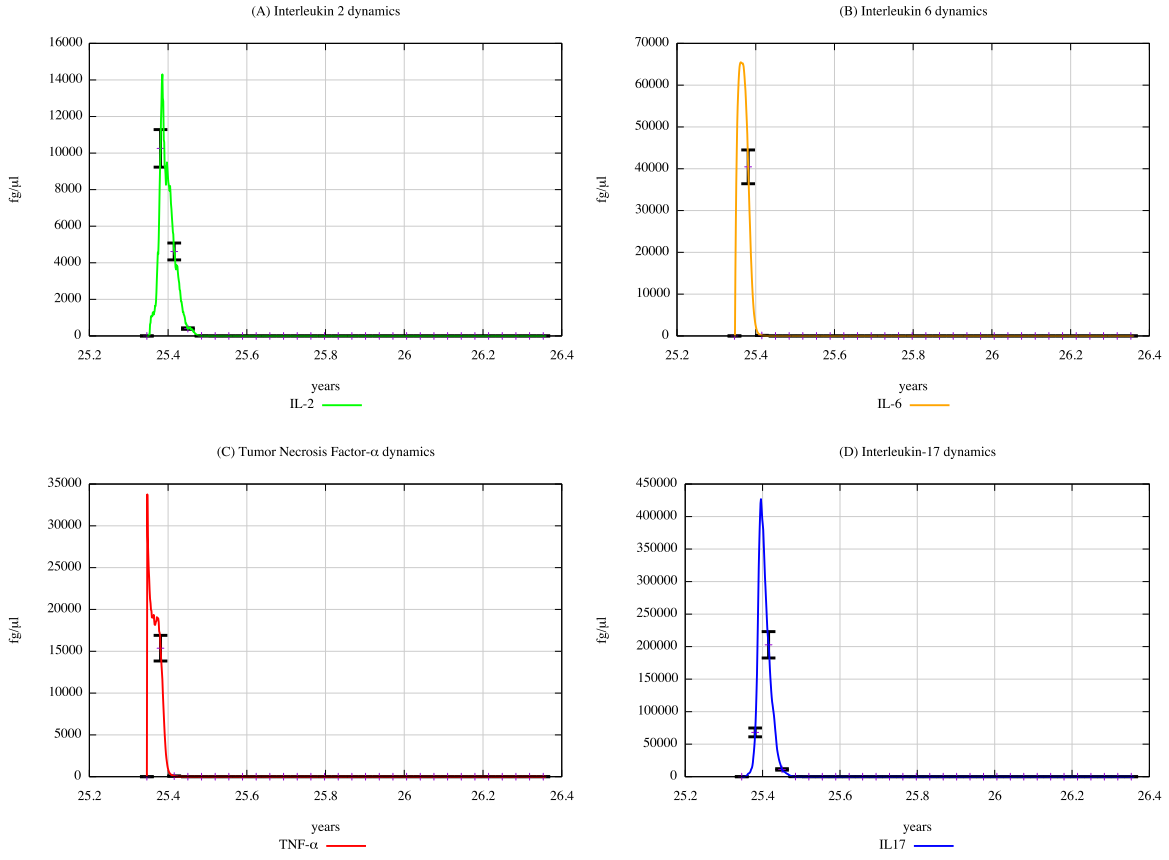

Fig. 11. Cytokines dynamics prediction for a digital cohort having an age range of 25–26 years and exposed to PFOA and PFOS according to "scenario 3".

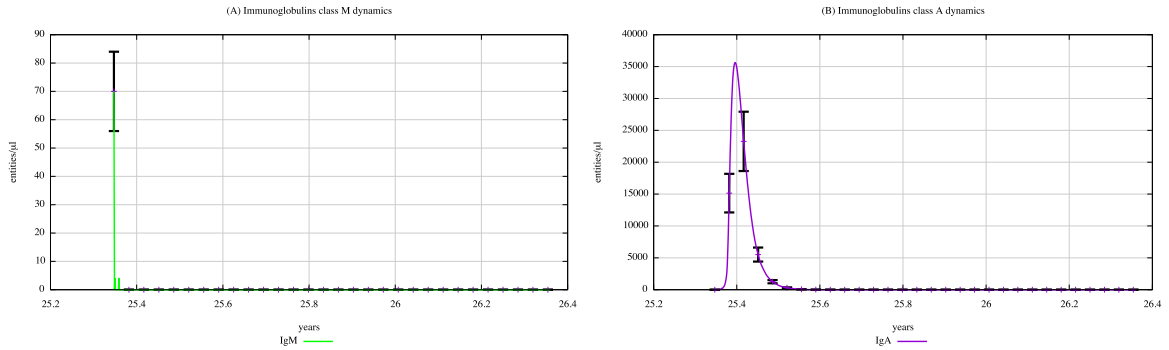

Fig. 12. Immunoglobulins dynamics prediction for "not exposed" scenario, age range 25–26 years.

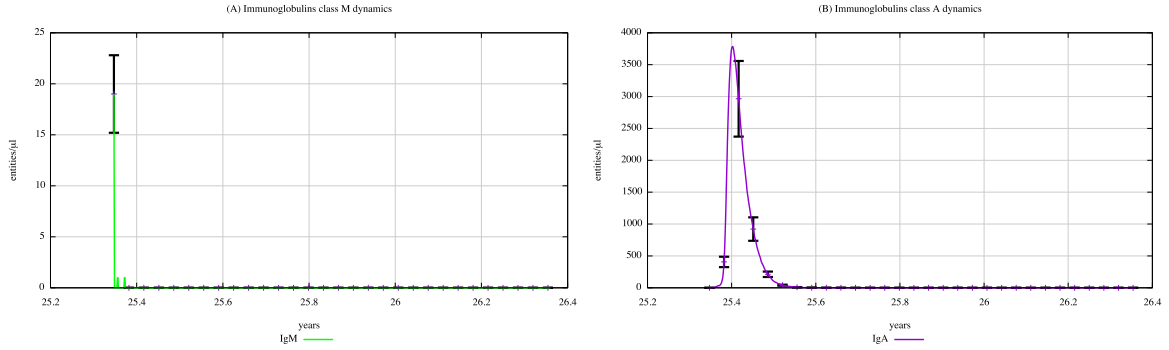

Fig. 13. Immunoglobulins dynamics prediction for a digital cohort having an age range of 25–26 years and exposed to PFOA and PFOS according to "scenario 3".

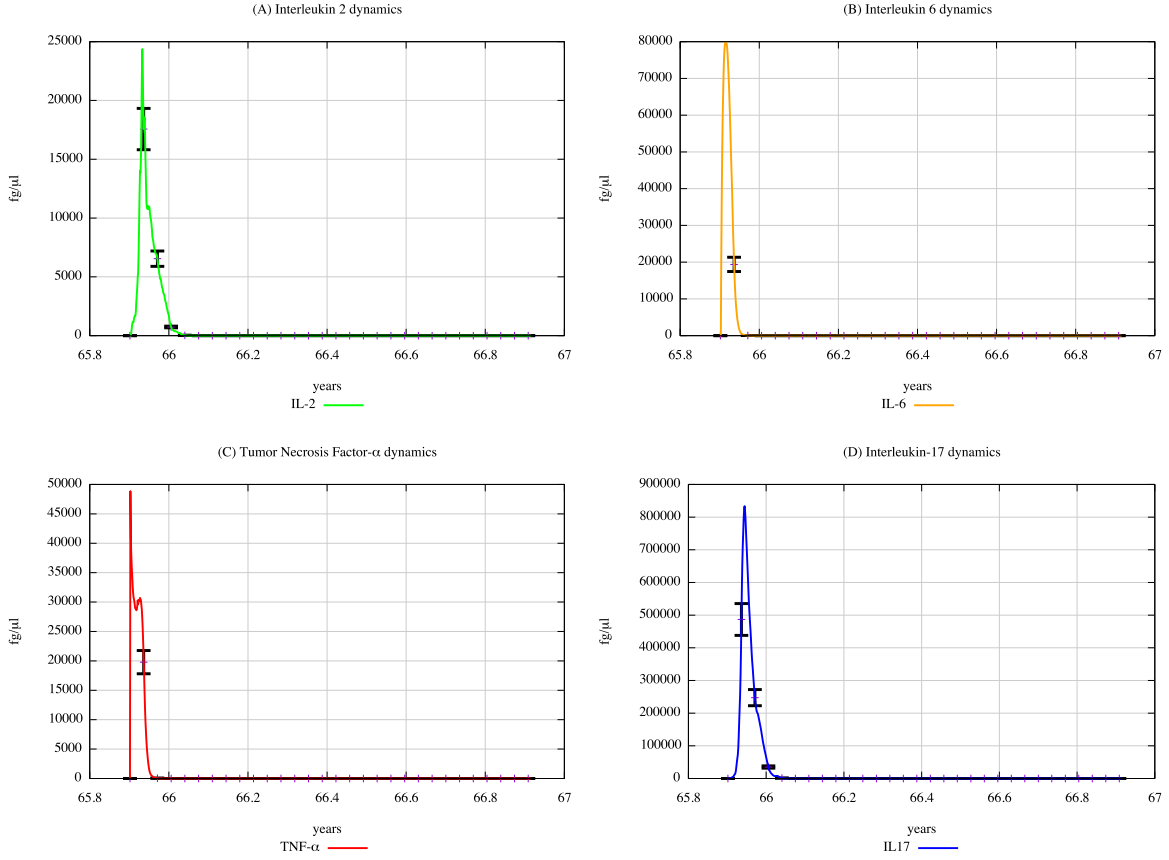

Fig. 14. Cytokines dynamics prediction for "not exposed" scenario, age range 65–66 years.

people and exposed ones according to "scenario 3″, respectively. In Supplementary Materials, plots depicting immunoglobulin dynamics in scenarios 1 and 2 are also shown. Comparing Figs. 12 and 13, we can notice a substantial reduction in IgM levels when digital patients are exposed to a high dose of PFOA and PFOS, demonstrating that the perfluoroalkyl substances have a role in reducing the immune system activity in terms of humoral response.

– 65-66 years (elderlies)

UISS can simulate the immune response also considering the age of digital patients. We simulated the immune response following a bacterial challenge in subjects aged 65 to 66 years, both unexposed and previously exposed to different concentrations of PFOA and PFOS (i.e. the three scenarios from the PBK model). Several plots depicting cytokines, immunoglobulins, and T- and B-cells dynamics were obtained. Here, the cytokines and the IgM and IgA dynamics in unexposed elderlies and in exposed ones according to the "scenario 3″ are shown. Results for scenarios 1 and 2, as well as on the T- and B-cells dynamics, are presented in Supplementary Materials.

From the comparison of Fig. 15 (PFOA and PFOS exposure) with Fig. 14 (PFAS not exposure), one can appreciate that the cytokine concentration levels gradually decrease along with in the three scenarios, except for the IL-2 and IL-6 levels observed in scenario 1 (results presented in Supplementary Materials).

Comparing Fig. 17 (PFOA and PFOS exposure) with Fig. 16 (PFAS not exposure), one can appreciate that the immunoglobulins concentration levels will gradually decrease along with the age for the three scenarios. In particular, based on the IgM and IgA dynamics, a strong reduction in their concentration can be observed when elderlies are previously exposed to PFOA and PFOS.

To sum up, the young people cohort (25–26 years) seems to be the most affected by perfluoroalkyl substances exposure. Indeed, we can observe a significant reduction in terms of immunological parameters, especially for the cytokine concentration levels (IL-2, IL-6, TNF-α, and IL-17) and B and CD4 + cell dynamics (activated Th17 and Th17 memory cells) for this cohort exposed to PFOA and PFOS according to scenario 3 (results are shown in Supplementary Materials).

In addition, a relevant reduction of immunoglobulins (particularly, IgM and IgA) was observed in both the elderly cohort (65–66 years) and in the children one (0–4 years) exposed to PFOA and PFOS according to scenario 3, along with a decrease in B cell dynamics (activated and memory B cells, shown in Supplementary Materials).

3.4. *Immune response after H1N1 and diphteria vaccines*

According to the three different exposure scenarios, we simulated and predicted the antibody response after anti-diphtheria and anti-H1N1 vaccine administration in a cohort of young people (25–26 years) and a cohort of 100 children (0–10 age range), respectively. We evaluated the antibody levels after the vaccine administration in the *in silico* cohorts previously exposed to PFOA and PFOS according to the three scenarios.

As we can see in Fig. 18, in the *in silico* cohort of 100 young people (25–26 age range) we observed a marked reduction in terms of vaccine response for scenario 3 after an anti-H1N1 challenge.

As Fig. 19 shows, in the *in silico* cohort of 100 children (0–10 age range), one can observe a marked reduction in terms of vaccine response in scenario 3 after the second challenge of the anti-diphtheria vaccine, according to the conventional vaccination schedule.

These results show that exposure to PFOA and PFOS, in particular considering scenario 3, causes a reduction in the immune response both in the cohort of young people and in the cohort of children, in agreement with previous findings showing reduced antibody production following

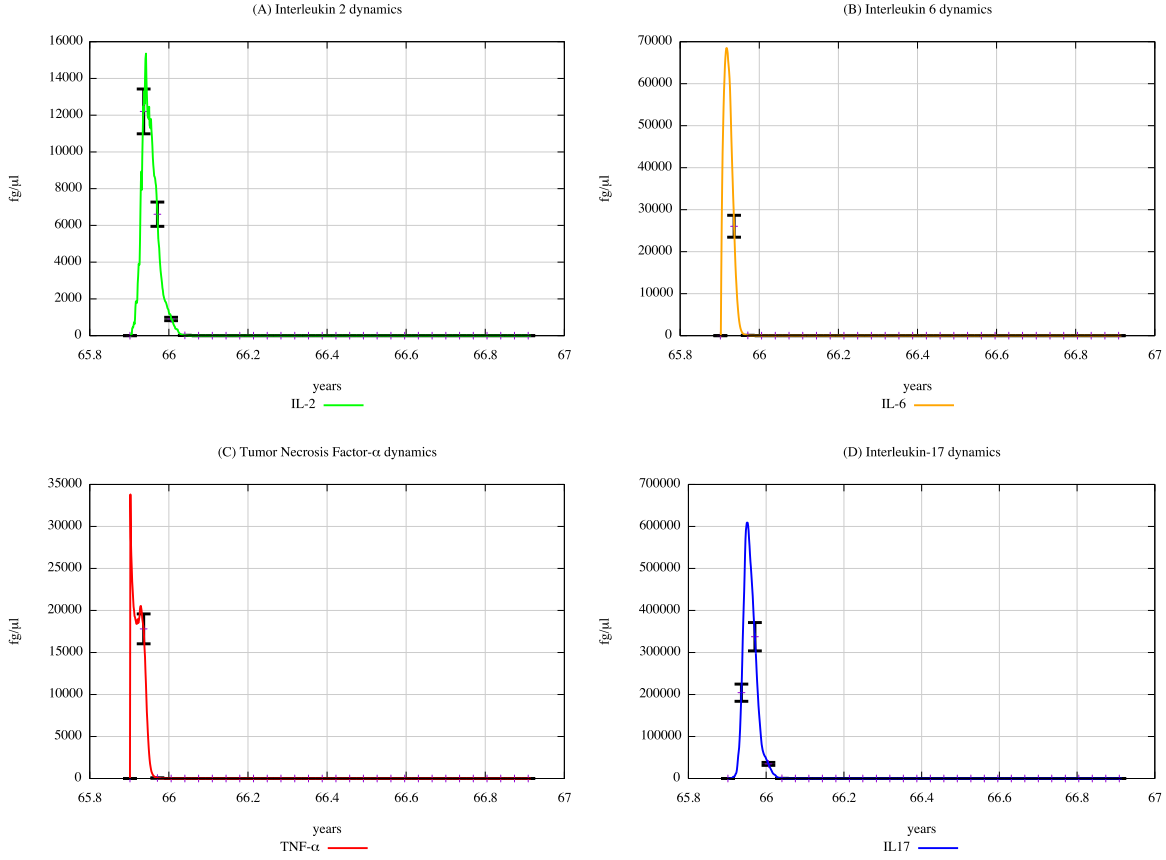

Fig. 15. Cytokines dynamics prediction for a digital cohort having an age range of 65–66 years and exposed to PFOA and PFOS according to "scenario 3″.

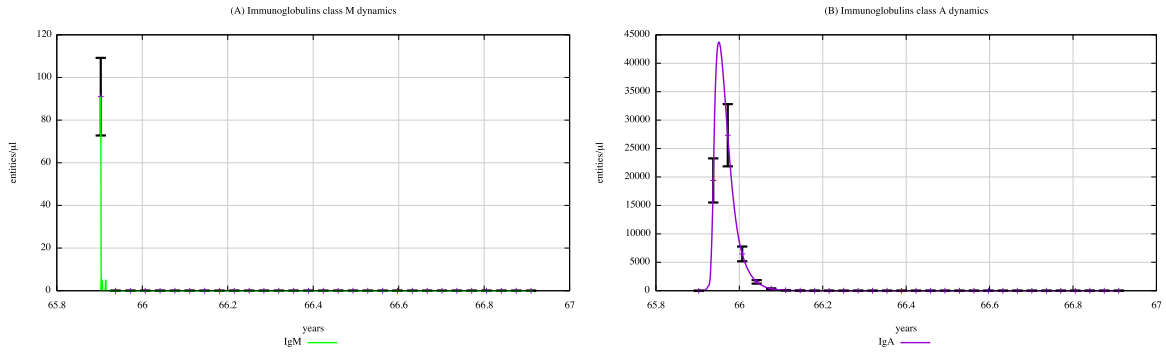

Fig. 16. Immunoglobulins dynamics prediction for "not exposed" scenario, age range 65–66 years.

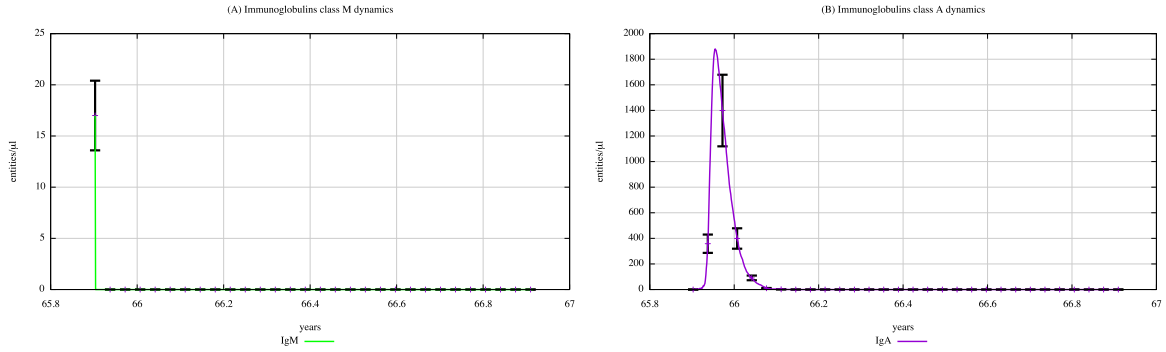

Fig. 17. Immunoglobulins dynamics prediction for a digital cohort having an age range of 64–65 years and exposed to PFOA and PFOS according to "scenario 3".

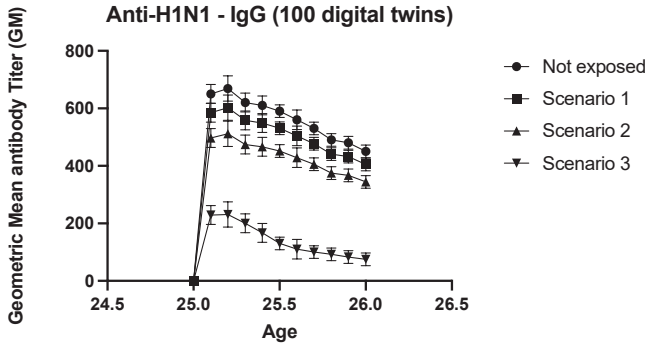

Fig. 18. Predicted anti-H1N1 antibodies titers of *in silico* patient cohorts exposed to the three different concentrations of PFOA and PFOS after having received influenza vaccination.

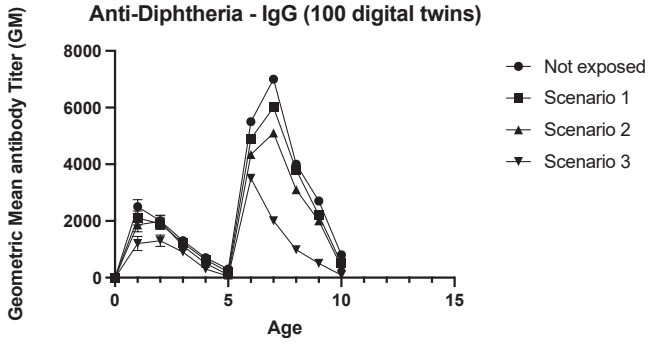

Fig. 19. Predicted anti-Diphtheria antibodies titers of *in silico* patient cohorts exposed to the three different concentrations of PFOA and PFOS after having received diphtheria vaccination.

the administration of vaccines [11,46].

4. Discussion

In summary, the study used advanced computational tools, including ABM, UISS, and PBK models, to gain a deeper understanding of the complex mechanisms of PFAS. PBK models have been employed to unravel the biokinetics of PFAS in the body, tracking absorption, distribution, metabolism and elimination at different dosage levels over the course of a person's life. While the adapted UISS has been instrumental in simulating host immune system responses to various stimuli in specific adverse healthcare settings, aiding chemical risk assessments. The aim was to develop an integrated approach capable of improving the predictive capabilities of the UISS-TOX model.

The existing PFAS PBK models were applied here under a number of different exposure scenarios. No PBK model development was performed under the present work. The presented results illustrate how the increasing concentration of oral exposure correlates with the increasing accumulation of PFAS in blood plasma. This is also in line with the half-lives in humans of PFAS that is 3.4 years for PFOS, 2.7 years for PFOA [43], 3.2 years for PFNA and 8.2 years for PFHxS [27,28]. Simulations for the four PFAS were selected for different oral exposure concentrations and the CA at different timing of exposure (every 8 h for 75 years) was taken to inform the UISS.

UISS simulated and predicted the effect of the two considered PFAS on the immune system, considering both the level of exposure and the age range of the *in silico* cohorts. The three *in silico* cohorts consisted of children (age range 0–4 years old), young people (age range 25–26 years old), and elderlies (age range 65–66 years old). Specifically, UISS predicted the effect of PFOA and PFOS on the immune system response in terms of cytokines, immunoglobulins (particularly IgM and IgA), and B- and T-cells dynamics, thus taking into account both cellular and humoral immune response.

UISS showed that the higher the exposure to PFAS, the lower the

production of cytokines, immunoglobulins, and B and T cell activity. In particular, the young people cohort (25–26 years) seems to be the most affected by perfluoroalkyl substances exposure, according to the significant reduction in immunological parameters, especially for the cytokine concentration levels and B and CD4 + cell dynamics in the exposed people according to scenario 3. Furthermore, evaluating the antibody levels, UISS simulated the effect of PFOA and PFOS exposure on the immune response to two different vaccine administrations. In an *in silico* cohort of 100 young people (25–26 years old), we observed a marked reduction in vaccine response for scenario 3 after an anti-H1N1 challenge. Similarly, in an *in silico* cohort of 100 children (0–10 age range), we observed a marked reduction in vaccine response in scenario 3 after the second challenge of the anti-diphtheria vaccine. Finally, exposure to PFOA and PFOS induced a reduced antibody response and, therefore, suppressed the immune response to vaccines in both cohorts.

For PFOA and PFOS the existing human PBK models were used as adapted by EFSA (EFSA 2020). The same models with slight modifications were applied here (in accordance with Fragki et al., 2023) to describe the kinetics of PFNA and PFHxS, based on data on their reported elimination half-lives. It shall be noted that because of the absence of suitable human biomonitoring data, the PFNA and PFHxS models were not verified directly on such data [27]. No PBK model development was performed as part of the present study. In the applied PBK models, only renal re-absorption has been investigated, while there is presently no available published PBK model describing the enterohepatic circulation of PFAS. However, works in this area are ongoing, in fact a PBK model is currently being developed by Husoy T and group, where the EFSA 2020 PBK model is extensively revisited to capture enterohepatic circulation using human biomonitoring data [47].

The PBK models applied do not include a clear representation of the immune system (e.g. alymph node compartment) as, for example, recently published for Bisphenol A by Loizou et al. [48]. Consequently, the blood levels were used as a proxy for immune system exposure. Adding such a lymph node compartment will provide a better way of connecting the kinetic PBK model to the dynamic UISS model. However, this would mean pre-parametrization and evaluation for which data are lacking.

5. Conclusions

Employing PBK and UISS models, this research harnessed the strengths of both *in silico* approaches to investigate impact of PFAS on the immune system, spotlighting the nuanced immune responses across different age groups. PBK model outcomes aligned well with existing data reporting PFAS concentration and accumulation patterns in the plasma, corroborating the noted extended half-lives of PFAS in humans, and demonstrating the robustness of the approach. Moreover, the detailed time-concentration profiles generated by the PBK model were pivotal in enhancing the predictive acumen of the UISS-TOX model.

The UISS simulations, which included distinct *in silico* cohorts – children (0–4 years), young adults (25–26 years), and elderly individuals (65–66 years), revealed significant alterations in immune response parameters including cytokine production, immunoglobulin levels (specifically IgM and IgA), and B- and T-cell dynamics. Notably, young adults appeared to bear the brunt of PFAS exposure, showcasing a pronounced dip in various immunological parameters, particularly under the simulated conditions of scenario 3, thereby accentuating concerns over potential heightened vulnerability of this demographic. Additionally, these models highlighted a disturbing trend of diminished vaccine efficacy against both H1N1 and diphtheria challenges in high-exposure scenarios, underscoring a suppressed immune responsiveness to vaccinations in affected cohorts.

Despite the promising insights garnered, it is acknowledged that the current PBK model lacks representation of the lymph node compartment, a critical component in connecting kinetic and dynamic models, thereby highlighting an avenue for further refinement and research. Moreover, the study pointed towards the necessity of exploring the enterohepatic circulation of PFAS, an aspect not encapsulated in existing PBK models, but which is currently under investigation by other research groups. The present findings call for further research and data to refine existing models and deepen our understanding of PFAS impacts on human health. In essence, this study forges a critical pathway towards more nuanced and comprehensive considerations to be used within risk assessment strategies, potentially supporting future policy frameworks and risk mitigations for PFAS exposures.

This comprehensive and integrative approach significantly bolsters the application of new approach methodologies in the field of risk assessment and in that specific case give us a promising direction in advancing our understanding of the hazardous impacts of PFAS on public health. This innovative approach not only stands as a potential bridge to existing data gaps but also encourages the exploration of complex mechanisms and the identification of unanticipated dynamics related to PFAS exposure. Consequently, it plays a pivotal role in enhancing our capacity for effective risk mitigation and in informing regulatory decisions. As we venture further into this frontier, it becomes increasingly plausible to facilitate more informed risk assessment, regulatory decisions and develop sound risk mitigation measures, thereby safeguarding the future from the adverse impacts of PFAS exposure. Furthermore, these insights lay the groundwork for further research, potentially guiding the development of strategies to mitigate human health impacts of these persistent compounds. In conclusion this advancement not only underscores the importance of embracing technological innovation in environmental health sciences but also highlights the potential for such tools to transform our approach to managing and regulating chemical risks in a manner that is both more informed and nuanced.

Funding

This study was supported by the European Food Safety Authority (Case Studies NAMS_PFAS Immunotox - OC/EFSA/SCER/2021/13).

CRediT authorship contribution statement

Martina Iulini: Writing – review & editing, Project administration, Methodology, Conceptualization. **Styliani Fragki:** Writing – review & editing. **Emanuela Corsini:** Writing – review & editing. **Francesco Pappalardo:** Writing – review & editing, Writing – original draft, Supervision, Methodology, Conceptualization. **Alicia Paini:** Writing – review & editing. **Giulia Russo:** Writing – review & editing, Methodology, Conceptualization. **Elena Crispino:** Writing – review & editing, Methodology.

Declaration of Competing Interest

Author Alicia Paini was employed by esqLABS GmbH, Saterland, Germany. The remaining authors declare that the research was conducted in the absence of any commercial or financial relationships that could be construed as a potential conflict of interest.

Acknowledgments

The authors wish to thank the EFSA Tender coordinators, and all the other people involved in the consortium for their work and scientific support: Jean-Lou Christian Michel Dorne, Chantra Eskes, Maria Chiara Astuto, Irene Cattaneo, Ambra Maddalon, Valentina Galbiati, Karsten Beekmann, Aafke Janseen and Ron Hoogenboom.

Appendix A. Supporting information

Supplementary data associated with this article can be found in the online version at doi:10.1016/j.csbj.2024.06.036.

References

[1] EFSA Panel on Contaminants in the Food Chain (EFSA CONTAM Panel), Schrenk D, Bignami M, Bodin L, Chipman JK, del Mazo J, Grasl-Kraupp B, et al. Risk to human health related to the presence of perfluoroalkyl substances in food. EFSA J 2020; 18. https://doi.org/10.2903/j.efsa.2020.6223.

[2] Fragki S, Dirven H, Fletcher T, Grasl-Kraupp B, Bjerve Gützkow K, Hoogenboom R, et al. Systemic PFOS and PFOA exposure and disturbed lipid homeostasis in humans: what do we know and what not. Crit Rev Toxicol 2021;51:141–64. https://doi.org/10.1080/10408444.2021.1888073.

[3] Trudel D, Horowitz L, Wormuth M, Scheringer M, Cousins IT, Hungerbühler K. Estimating consumer exposure to PFOS and PFOA. Risk Anal 2008;28:251–69. https://doi.org/10.1111/j.1539-6924.2008.01017.x.

[4] Harada KH, Hashida S, Kaneko T, Takenaka K, Minata M, Inoue K, et al. Biliary excretion and cerebrospinal fluid partition of perfluorooctanoate and perfluorooctane sulfonate in humans. Environ Toxicol Pharmacol 2007;24:134–9. https://doi.org/10.1016/j.etap.2007.04.003.

[5] Fujii Y, Niisoe T, Harada KH, Uemoto S, Ogura Y, Takenaka K, et al. Toxicokinetics of perfluoroalkyl carboxylic acids with different carbon chain lengths in mice and humans. J Occup Health 2015;57:1–12. https://doi.org/10.1539/joh.14-0136-OA.

[6] Nakagawa H, Hirata T, Terada T, Jutabha P, Miura D, Harada KH, et al. Roles of organic anion transporters in the renal excretion of perfluorooctanoic acid. Basic Clin Pharmacol Toxicol 2008;103:1–8. https://doi.org/10.1111/j.1742-7843.2007.00155.x.

[7] Han X, Nabb DL, Russell MH, Kennedy GL, Rickard RW. Renal elimination of perfluorocarboxylates (PFCAs). Chem Res Toxicol 2012;25:35–46. https://doi.org/10.1021/tx200363w.

[8] Louisse J, Dellafiora L, Van Den Heuvel JJMW, Rijkers D, Leenders L, Dorne J-LCM, et al. Perfluoroalkyl substances (PFASs) are substrates of the renal human organic anion transporter 4 (OAT4). Arch Toxicol 2023;97:685–96. https://doi.org/10.1007/s00204-022-03428-6.

[9] Li Y, Fletcher T, Mucs D, Scott K, Lindh CH, Tallving P, et al. Half-lives of PFOS, PFHxS and PFOA after end of exposure to contaminated drinking water. Occup Environ Med 2018;75:46–51. https://doi.org/10.1136/oemed-2017-104651.

[10] Corsini E, Luebke RW, Germolec DR, DeWitt JC. Perfluorinated compounds: emerging POPs with potential immunotoxicity. Toxicol Lett 2014;230:263–70. https://doi.org/10.1016/j.toxlet.2014.01.038.

[11] Abraham K, Mielke H, Fromme H, Völkel W, Menzel J, Peiser M, et al. Internal exposure to perfluoroalkyl substances (PFASs) and biological markers in 101 healthy 1-year-old children: associations between levels of perfluorooctanoic acid (PFOA) and vaccine response. Arch Toxicol 2020;94:2131–47. https://doi.org/10.1007/s00204-020-02715-4.

[12] Kielsen K, Shamim Z, Ryder LP, Nielsen F, Grandjean P, Budtz-Jørgensen E, et al. Antibody response to booster vaccination with tetanus and diphtheria in adults exposed to perfluorinated alkylates. J Immunotoxicol 2016;13:270–3. https://doi.org/10.3109/1547691X.2015.1067259.

[13] Dalsager L, Christensen N, Halekoh U, Timmermann CAG, Nielsen F, Kyhl HB, et al. Exposure to perfluoroalkyl substances during fetal life and hospitalization for infectious disease in childhood: a study among 1,503 children from the Odense Child Cohort. Environ Int 2021;149:106395. https://doi.org/10.1016/j.envint.2021.106395.

[14] Averina M, Brox J, Huber S, Furberg A-S, Sørensen M. Serum perfluoroalkyl substances (PFAS) and risk of asthma and various allergies in adolescents. The Tromsø study Fit Futures in Northern Norway. Environ Res 2019;169:114–21. https://doi.org/10.1016/j.envres.2018.11.005.

[15] Buser MC, Scinicariello F. Perfluoroalkyl substances and food allergies in adolescents. Environ Int 2016;88:74–9. https://doi.org/10.1016/j.envint.2015.12.020.

[16] Russo G, Crispino E, Corsini E, Iulini M, Paini A, Worth A, et al. Computational modelling and simulation for immunotoxicity prediction induced by skin sensitisers. Comput Struct Biotechnol J 2022;20:6172–81. https://doi.org/10.1016/j.csbj.2022.10.032.

[17] Pappalardo F, Russo G, Corsini E, Paini A, Worth A. Translatability and transferability of in silico models: Context of use switching to predict the effects of environmental chemicals on the immune system. Comput Struct Biotechnol J 2022; 20:1764–77. https://doi.org/10.1016/j.csbj.2022.03.024.

[18] Rietjens IMCM, Louisse J, Punt A. Tutorial on physiologically based kinetic modeling in molecular nutrition and food research. Mol Nutr Food Res 2011;55: 941–56. https://doi.org/10.1002/mnfr.201000655.

[19] Kuepfer L, Niederalt C, Wendl T, Schlender J, Willmann S, Lippert J, et al. Applied concepts in PBPK modeling: how to build a PBPK/PD model. CPT Pharmacomet Syst Pharmacol 2016;5:516–31. https://doi.org/10.1002/psp4.12134.

[20] Bois FY, Jamei M, Clewell HJ. PBPK modelling of inter-individual variability in the pharmacokinetics of environmental chemicals. Toxicology 2010;278:256–67. https://doi.org/10.1016/j.tox.2010.06.007.

[21] Clewell RA, Clewell HJ. Development and specification of physiologically based pharmacokinetic models for use in risk assessment. Regul Toxicol Pharmacol 2008; 50:129–43. https://doi.org/10.1016/j.yrtph.2007.10.012.

[22] Hartung T. Perspectives on *In Vitro* to *In Vivo* extrapolations. Appl Vitr Toxicol 2018;4:305–16. https://doi.org/10.1089/aivt.2016.0026.

[23] Louisse J, Beekmann K, Rietjens IMCM. Use of physiologically based kinetic modeling-based reverse dosimetry to predict in vivo toxicity from in vitro data. Chem Res Toxicol 2017;30:114–25. https://doi.org/10.1021/acs.chemrestox.6b00302.

[24] Thompson CV, Firman JW, Goldsmith MR, Grulke CM, Tan Y-M, Paini A, et al. A systematic review of published physiologically-based kinetic models and an assessment of their chemical space coverage. Altern Lab Anim 2021;49:197–208. https://doi.org/10.1177/02611929211060264.

[25] Loccisano AE, Campbell JL, Andersen ME, Clewell HJ. Evaluation and prediction of pharmacokinetics of PFOA and PFOS in the monkey and human using a PBPK model. Regul Toxicol Pharmacol 2011;59:157–75. https://doi.org/10.1016/j.yrtph.2010.12.004.

[26] Fragki S, Louisse J, Bokkers B, Luijten M, Peijnenburg A, Rijkers D, et al. New approach methodologies: a quantitative in vitro to in vivo extrapolation case study with PFASs. Food Chem Toxicol 2023;172:113559. https://doi.org/10.1016/j.fct.2022.113559.

[27] Olsen GW, Burris JM, Ehresman DJ, Froehlich JW, Seacat AM, Butenhoff JL, et al. Half-life of serum elimination of perfluorooctanesulfonate, perfluorohexanesulfonate, and perfluorooctanoate in retired fluorochemical production workers. Environ Health Perspect 2007;115:1298–305. https://doi.org/10.1289/ehp.10009.

[28] Zhang Y, Beesoon S, Zhu L, Martin JW. Biomonitoring of perfluoroalkyl acids in human urine and estimates of biological half-life. Environ Sci Technol 2013;47: 10619–27. https://doi.org/10.1021/es401905e.

[29] EFSA Panel on Contaminants in the Food Chain (CONTAM), Knutsen HK, Alexander J, Barregård L, Bignami M, Brüschweiler B, Ceccatelli S, et al. Risk to human health related to the presence of perfluorooctane sulfonic acid and perfluorooctanoic acid in food. EFSA J 2018;16. https://doi.org/10.2903/j.efsa.2018.5194.

[30] Holmquist H, Fantke P, Cousins IT, Owsianiak M, Liagkouridis I, Peters GM. An (eco)toxicity life cycle impact assessment framework for per- and polyfluoroalkyl substances. Environ Sci Technol 2020;54:6224–34. https://doi.org/10.1021/acs.est.9b07774.

[31] Schlüter U, Meyer J, Ahrens A, Borghi F, Clerc F, Delmaar C, et al. Exposure modelling in Europe: how to pave the road for the future as part of the European Exposure Science Strategy 2020–2030. J Expo Sci Environ Epidemiol 2022;32: 499–512. https://doi.org/10.1038/s41370-022-00455-4.

[32] Ericson I, Gómez M, Nadal M, Van Bavel B, Lindström G, Domingo JL. Perfluorinated chemicals in blood of residents in Catalonia (Spain) in relation to age and gender: a pilot study. Environ Int 2007;33:616–23. https://doi.org/10.1016/j.envint.2007.01.003.

[33] Pérez F, Nadal M, Navarro-Ortega A, Fàbrega F, Domingo JL, Barceló D, et al. Accumulation of perfluoroalkyl substances in human tissues. Environ Int 2013;59: 354–62. https://doi.org/10.1016/j.envint.2013.06.004.

[34] Fàbrega F, Kumar V, Schuhmacher M, Domingo JL, Nadal M. PBPK modeling for PFOS and PFOA: validation with human experimental data. Toxicol Lett 2014;230: 244–51. https://doi.org/10.1016/j.toxlet.2014.01.007.

[35] Bartell SM, Calafat AM, Lyu C, Kato K, Ryan PB, Steenland K. Rate of decline in serum PFOA concentrations after granular activated carbon filtration at two public water systems in Ohio and West Virginia. Environ Health Perspect 2010;118: 222–8. https://doi.org/10.1289/ehp.0901252.

[36] Kudo N, Sakai A, Mitsumoto A, Hibino Y, Tsuda T, Kawashima Y. Tissue distribution and hepatic subcellular distribution of perfluorooctanoic acid at low dose are different from those at high dose in rats. Biol Pharm Bull 2007;30: 1535–40. https://doi.org/10.1248/bpb.30.1535.

[37] Harada K, Inoue K, Morikawa A, Yoshinaga T, Saito N, Koizumi A. Renal clearance of perfluorooctane sulfonate and perfluorooctanoate in humans and their species-specific excretion. Environ Res 2005;99:253–61. https://doi.org/10.1016/j.envres.2004.12.003.

[38] National Toxicology Program., Toxicity studies of perfluoroalkyl carboxylates administered by gavage to Sprague Dawley, (2019). ⟨https://doi.org/10.22427/NTP-TOX-97⟩.

[39] R. Macey, G. Oster, T. Zahnley, Berkeley Madonna User's Guide, (n.d.).

[40] Arnich N, Sirot V, Rivière G, Jean J, Noël L, Guérin T, et al. Dietary exposure to trace elements and health risk assessment in the 2nd French Total Diet Study. Food Chem Toxicol 2012;50:2432–49. https://doi.org/10.1016/j.fct.2012.04.016.

[41] Ebrahim GJ. WHO Child Growth Standards. Growth Velocity Based on Weight, Length and Head Circumference. * Methods and Development. 136–136 J Trop Pediatr 2010;56. https://doi.org/10.1093/tropej/fmp086.

[42] Brown RP, Delp MD, Lindstedt SL, Rhomberg LR, Beliles RP. Physiological parameter values for physiologically based pharmacokinetic models. Toxicol Ind Health 1997;13:407–84. https://doi.org/10.1177/074823379701300401.

[43] Li Y, Barregard L, Xu Y, Scott K, Pineda D, Lindh CH, et al. Associations between perfluoroalkyl substances and serum lipids in a Swedish adult population with contaminated drinking water. Environ Health 2020;19:33. https://doi.org/10.1186/s12940-020-00588-9.

[44] Nian M, Zhou W, Feng Y, Wang Y, Chen Q, Zhang J. Emerging and legacy PFAS and cytokine homeostasis in women of childbearing age. Sci Rep 2022;12:6517. https://doi.org/10.1038/s41598-022-10501-8.

[45] Neagu M, Constantin C, Bardi G, Duraes L. Adverse outcome pathway in immunotoxicity of perfluoroalkyls. Curr Opin Toxicol 2021;25:23–9. https://doi.org/10.1016/j.cotox.2021.02.001.

[46] Grandjean P, Andersen EW, Budtz-Jørgensen E, Nielsen F, Mølbak K, Weihe P, et al. Serum vaccine antibody concentrations in children exposed to perfluorinated compounds. JAMA 2012;307. https://doi.org/10.1001/jama.2011.2034.

[47] Husøy T, Martínez MA, Sharma RP, Kumar V, Andreassen M, Sakhi AK, et al. Comparison of aggregated exposure to di(2-ethylhexyl) phthalate from diet and personal care products with urinary concentrations of metabolites using a PBPK model – Results from the Norwegian biomonitoring study in EuroMix. Food Chem Toxicol 2020;143:111510. https://doi.org/10.1016/j.fct.2020.111510.

[48] Loizou G, McNally K, Paini A, Hogg A. Derivation of a human in vivo benchmark dose for bisphenol A from ToxCast in vitro concentration response data using a

computational workflow for probabilistic quantitative in vitro to in vivo extrapolation. Front Pharmacol 2022;12:754408. https://doi.org/10.3389/fphar.2021.754408.